VIRGINIA POLYTECHNIC INSTITUTE
AND STATE UNIVERSITY

The Charles E. Via, Jr. Department
of Civil and Environmental Engineering
Blacksburg, VA 24061

Structural Engineering and Materials

DISTORTIONAL BUCKLING EXPERIMENTS ON COLD-FORMED STEEL JOISTS WITH UNSTIFFENED HOLES

by
Anna Schudlich
Visiting Student Scholar

Aaron von der Heyden
Visiting Student Scholar

Cristopher D. Moen, Ph.D., P.E.

Report No. CE/VPI-ST-11/05

September 2011

DISTORTIONAL BUCKLING EXPERIMENTS ON COLD-FORMED STEEL JOISTS WITH UNSTIFFENED HOLES

Anna Schudlich[a], Aaron von der Heyden[b], Cristopher D. Moen[c]

[a,b] *Technische Universität Darmstadt, Darmstadt, DE*
[c] *Virginia Tech, Blacksburg, Virginia, USA*

Abstract: Experiments were conducted on cold-formed steel C-section joists with rectangular unstiffened web holes. The presence of holes decreased joist capacity and amplified distortional buckling deformation. Distortional buckling was accompanied by unstiffened strip buckling of the compressed web. When hole depth approached the web depth, sudden flexural buckling of the compressed flange at the hole was observed. Forthcoming direct strength method equations for joists with holes accurately predicted flexural capacity when web hole depth equaled two-thirds the web depth, and was unconservative for larger web holes.

1. INTRODUCTION

Distortional buckling is a strength limit state in cold-formed steel joists with open cross-sections, e.g., a Z-section or a C-section, where the compressed flange rotates about the flange-web intersection in restrained flexural-torsional buckling [1]. The web provides rotational restraint to the compressed flange, and therefore the web bending stiffness influences elastic distortional buckling parameters and distortional buckling capacity.

When discrete holes (perforations) are placed in the web of cold-formed steel joists to accommodate ventilation, plumbing, or electrical conduits, the rotational stiffness provided by the web to the flange is interrupted, and the critical elastic distortional buckling moment, M_{crd}, decreases [2]. If the distortional buckling moment decreases, then with a direct strength (DSM) approach [3], it is hypothesized that distortional buckling capacity should also decrease. This strength trend has been observed in finite element simulations to collapse [4].

The goal of the research described herein is to explore experimentally the load-deformation response and capacity of cold-formed steel C-section joists with discrete unstiffened web holes. An industry standard cross-section susceptible to distortional buckling is selected, and hole depth is varied to evaluate how the loss in web material affects flexural capacity. Special attention is paid to the amplification of distortional buckling deformation with the presence of unstiffened holes, and the results are compared to forthcoming DSM equations for cold-formed steel flexural members with holes [5].

2. EXPERIMENTAL PROGRAM

2.1 Cross-section selection and specimen naming convention

A Structural Stud Manufacturers Association (SSMA) SSMA 800S250-68 cross-section was selected for this study because the predicted DSM distortional buckling capacity is lower than the local-global buckling capacity, i.e., $M_{nd} << M_{n\ell}$, and because inelastic distortional

buckling is expected, i.e., $\lambda_d=(M_y/M_{crd})^{0.5}\approx1$, which is a slenderness region where flexural capacity can be sensitive to the presence of holes. The nominal cross-section depth is 203 mm (8.00 in.), with 63 mm (2.50 in.) wide flanges and a nominal thickness of 1.7 mm (0.068 in.).

2.2 Test setup

Four point bending tests were performed in displacement control as shown in Fig. 1a. The specimens were oriented web to web and through bolted (4-13 mm diameter bolts per web) to HSS tubes at the third points and at the end supports (Fig. 1b). Scissor braces were used to laterally brace the spreader beam and the specimens at the loading points. Outside the constant moment region, the joist top and bottom flanges were fastened together with trapezoidal metal sheets (0.457 mm thickness) and self-tapping screws spaced at 300 mm on center.

2.3 Instrumentation

Load cells were located between plates at the top of the HSS tubes to measure the load in each specimen separately - 2 load cells at each load point for a total of 8 load cells. Linear variable differential transformers (LVDTs) measured vertical joist displacement at each load point. Additionally, 3 LVDTs per joist measured compression flange vertical (distortional) deflection at the midlength of each hole (Fig. 1a).

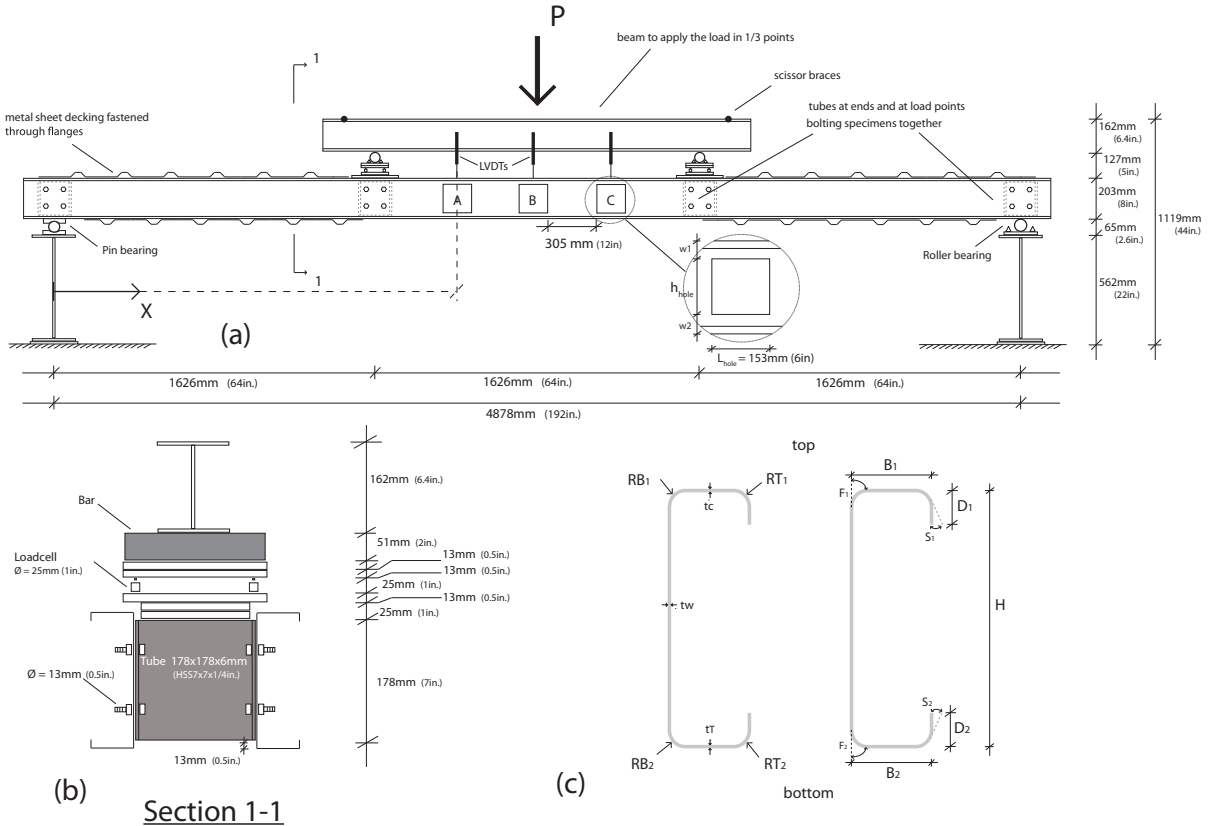

Fig. 1: (a) Test setup, (b) loading point, and (c) cross-section dimension notation

2.4 Specimen dimensions

The measured specimen cross-section dimensions are provided in Table 1, with Fig. 1c summarizing the dimension notation. Each joist had three rectangular holes centered transversely in the web and longitudinally along the joist between supports (Fig. 1a). The holes

were cut with a precision water jet system. Hole depth varies with the ratio of I_{net} to I_g, where I_{net} and I_g are the nominal net and gross strong axis centroidal moments of inertia. For I_{net}/I_g = 0.90, the nominal hole depth, h_{hole}, is 137mm, and for I_{net}/I_g = 0.80, h_{hole}=172mm. The measured hole dimensions after water jet cutting are summarized in Table 2.

All specimens were delivered with small vertical kinks distributed randomly along the joist length, which mostly liked occurred during the roll-forming process. The kinks extended vertically from the web into the C-section flanges and lips. All kink locations were measured, see [6] for details.

Table 1: Measured specimen cross-section dimensions and yield stress

Specimen	f_y [MPa]	t [mm]	H [mm]	B_1 [mm]	B_2 [mm]	D_1 [mm]	D_2 [mm]	F_1 [°]	F_2 [°]	S_1 [°]	S_2 [°]	RB_1 [mm]	RB_2 [mm]	RT_1 [mm]	RT_2 [mm]
800S250-68-NH-1.1	380	1.76	203.0	63.0	63.4	15.4	13.9	88.3	89.3	3.6	4.1	4.6	4.7	4.5	4.1
800S250-68-NH-1.2	363	1.77	203.2	62.8	63.4	15.3	14.0	87.6	89.9	4.0	3.7	4.7	5.5	4.9	4.4
800S250-68-NH-2.1	364	1.76	203.3	62.7	63.5	15.4	14.2	88.0	89.5	3.7	3.6	5.1	4.8	4.6	4.5
800S250-68-NH-2.2	375	1.78	203.1	62.7	63.5	15.2	14.0	86.5	89.3	3.9	4.1	4.9	4.7	4.9	4.2
800S250-68-NH-3.1	378	1.78	203.1	62.7	63.5	13.1	14.2	87.0	89.0	4.6	4.8	5.2	4.9	4.8	4.7
800S250-68-NH-3.2	371	1.77	203.0	62.7	63.4	15.3	14.1	87.7	89.0	3.8	3.5	4.7	4.9	4.2	3.9
800S250-68-H0.9-1.1	365	1.76	203.0	63.7	62.6	13.7	15.6	89.6	87.6	2.9	3.5	5.2	5.3	5.2	5.0
800S250-68-H0.9-1.2	366	1.77	203.0	62.7	63.5	15.5	13.8	87.7	90.1	3.7	3.6	5.3	5.2	4.8	5.0
800S250-68-H0.9-2.1	368	1.76	203.1	62.7	63.6	15.4	13.9	87.2	89.9	4.0	4.2	5.2	4.7	5.2	4.4
800S250-68-H0.9-2.2	363	1.77	203.1	62.6	63.6	15.3	13.9	87.9	89.9	4.3	3.3	5.4	4.7	5.1	4.8
800S250-68-H0.9-3.1	370	1.77	203.0	62.8	63.4	15.5	13.8	86.7	89.1	4.1	3.7	5.0	5.1	4.4	4.9
800S250-68-H0.9-3.2	369	1.78	202.9	62.8	63.4	15.6	13.6	86.7	89.6	3.4	3.8	5.2	5.3	4.7	4.3
800S250-68-H0.8-1.1	364	1.76	203.0	62.7	63.4	15.0	13.7	88.2	89.8	3.5	2.8	4.3	5.1	3.9	3.8
800S250-68-H0.8-1.2	360	1.77	203.0	63.5	62.9	14.0	15.2	89.8	87.1	3.3	4.3	4.7	5.4	4.7	4.5
800S250-68-H0.8-2.1	363	1.77	203.1	62.8	63.6	15.1	14.0	87.3	89.3	3.3	3.5	5.8	5.3	5.2	4.9
800S250-68-H0.8-2.2	363	1.75	203.1	63.5	62.7	14.3	15.3	89.7	87.3	3.0	4.0	5.2	5.1	4.4	4.7
800S250-68-H0.8-3.1	375	1.76	202.9	63.4	62.7	13.7	15.4	88.9	87.7	3.3	3.4	5.8	5.7	4.8	5.2
800S250-68-H0.8-3.2	376	1.76	203.1	63.4	62.6	14.0	15.2	89.7	87.3	3.6	3.6	4.4	5.7	4.7	4.4

Table 2: Measured hole dimensions and locations

Specimen	**Hole A**					**Hole B**					**Hole C**				
	X [mm]	L_{hole} [mm]	d_{hole} [mm]	w_1 [mm]	w_2 [mm]	X [mm]	L_{hole} [mm]	d_{hole} [mm]	w_1 [mm]	w_2 [mm]	X [mm]	L_{hole} [mm]	d_{hole} [mm]	w_1 [mm]	w_2 [mm]
800S250-68-H0.9-1.1	1980.3	152.3	136.6	32.5	33.3	2437.5	152.3	136.7	32.7	33.1	2894.7	152.3	136.7	32.6	33.1
800S250-68-H0.9-1.2	1980.3	152.3	136.7	33.5	31.8	2437.5	152.3	136.7	33.1	32.2	2894.7	152.3	136.8	33.0	32.6
800S250-68-H0.9-2.1	1980.3	152.3	136.7	33.0	32.6	2437.5	152.3	136.7	33.2	32.6	2894.7	152.4	136.7	33.3	32.4
800S250-68-H0.9-2.2	1980.3	152.4	136.7	32.8	32.8	2437.5	152.3	136.7	32.7	32.9	2894.7	152.3	136.7	32.4	33.3
800S250-68-H0.9-3.1	1980.3	152.3	136.7	32.4	33.3	2437.5	152.3	136.7	32.8	33.1	2894.7	152.3	136.7	32.9	32.8
800S250-68-H0.9-3.2	1980.3	152.4	136.6	33.4	32.3	2437.5	152.3	136.7	33.3	32.5	2894.7	152.4	136.7	33.2	32.6
800S250-68-H0.8-1.1	1980.3	152.1	172.1	15.4	14.9	2437.5	152.0	172.1	15.4	15.0	2894.7	152.0	171.9	15.4	15.3
800S250-68-H0.8-1.2	1980.3	151.9	172.2	14.9	15.3	2437.5	151.9	172.1	15.0	15.1	2894.7	152.1	172.0	15.1	14.9
800S250-68-H0.8-2.1	1980.3	151.8	172.1	15.5	14.9	2437.5	152.0	172.1	15.4	15.2	2894.7	152.1	171.8	15.3	15.4
800S250-68-H0.8-2.2	1980.3	152.1	172.0	14.9	15.5	2437.5	152.0	172.2	14.8	15.3	2894.7	152.0	171.9	15.0	15.6
800S250-68-H0.8-3.1	1980.3	152.0	172.0	14.6	15.9	2437.5	152.0	172.2	14.4	15.8	2894.7	152.1	172.3	14.5	15.6
800S250-68-H0.8-3.2	1980.3	151.9	172.2	14.6	15.6	2437.5	152.0	172.1	14.6	15.9	2894.7	152.0	171.8	14.8	15.8

2.5 Material properties

The steel yield stress was determined for the flanges and web in accordance with ASTM E8 [7]. All stress-strain curves demonstrated a sharp yielding plateau. The specimen yield stress, f_y, reported in Table 1 is the average of the yield stresses from the web and two flanges.

2.6 Test procedure

Each specimen was loaded with a hydraulic actuator at a displacement rate of 0.089 mm/s. Digital video of each test was recorded and is available on YouTube [8]. Data was recorded up to and beyond peak load to evaluate post-peak ductility and deformation patterns. See [6] for pictures and details of each experiment.

2.7 Test results

Tested capacities and failure modes are summarized in Table 3. In all tests, one joist in the pair failed first. Joist capacity was determined by evenly dividing the total actuator load (P/4 to each load point) at failure of the first joist. The joist that failed first is provided in Table 3. For example, joist 2 failed before joist 1 in test NH-3.2, and joist 1 failed before joist 2 in test NH-1.1.

All NH (no hole) specimens experienced an inelastic local buckling failure (Fig. 2), even though DSM predicted a distortional buckling failure. The local buckling failure location always initiated at one of the vertical kink imperfections from roll-forming (see Section 2.4).

The flexural capacity decreased by an average of 19% for joists with holes and I_{net}/I_g = 0.90. In 2 of the 3 tests at I_{net}/I_g = 0.90 (H.09-1.1, H.09-3.1), a distortional buckling failure was observed at a hole, accompanied by unstiffened strip buckling of the compressed web above the hole (Fig. 3). The distortional buckling pattern was always "up-down-up", with a loss in capacity occurring when the flange lip buckled in an "up" wave at the hole. The other specimen (H.09-2.2) failed from local unstiffened strip buckling at a hole without distortional buckling deformation. See [6] for pictures and details. The compression flange stiffening lip length for H.09-1.1 was 2 mm shorter than the H.09-2.2 and H.09-3.1 specimens, resulting in a 10% reduction in flexural capacity (compare 9.65 kN-m to 10.54 kN-m and 10.84 kN-m in Table 3).

Specimens with I_{net}/I_g = 0.80 experienced on average a 34% reduction in capacity when compared to the specimens without holes. In 2 of the 3 specimens, distortional buckling deformation was observed with large "up-down-up" displacements of the compression flange coincident with the holes, see Fig. 5c (H.08) and compare to Fig. 5a (NH) and Fig. 5b (H.09). These large distortional deformations resulted in buckling of the flange at the hole (Fig. 4), which was a different distortional buckling failure mode than in the H.09 specimens, where failure was concentrated in the stiffening lip and unstiffened strip above the hole. Buckling of the unstiffened strip above the hole was not observed in the H.08 specimens because it was narrow and therefore axially stiff [9]. The H.08.3.2 specimen failed when the compressed flange spanning between a hole suddenly collapsed in "local Euler" buckling (Fig. 6). For specimens with holes, the presence of the vertical kink imperfections did not influence failure mode or location.

Table 3: Tested flexural capacity

Specimen	M_y [kNm]	$M_{y,net}$ [kNm]	M_{test} [kNm]	M_{test} statistics	
				Mean [kNm]	C.o.V.
800S250-68-NH-1.1	13.77	-	12.60		
800S250-68-NH-2.1	13.45	-	12.51	12.71	0.02
800S250-68-NH-3.2	13.70	-	13.02		
800S250-68-H0.9-1.1	13.24	11.98	9.65		
800S250-68-H0.9-2.2	13.16	11.90	10.54	10.34	0.05
800S250-68-H0.9-3.1	13.39	12.32	10.84		
800S250-68-H0.8-1.2	13.22	10.67	8.19		
800S250-68-H0.8-2.2	13.18	10.66	8.55	8.43	0.02
800S250-68-H0.8-3.2	13.82	11.16	8.56		

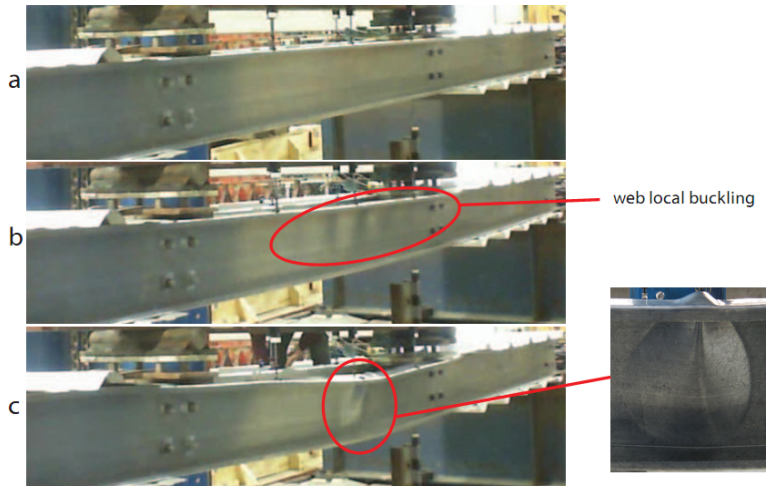

Fig. 2: Load-displacement progression for specimen NH-3.2 (a) M=0kNm, (b) M=13.02kNm (peak load) and (c) after collapse M=5.23kNm

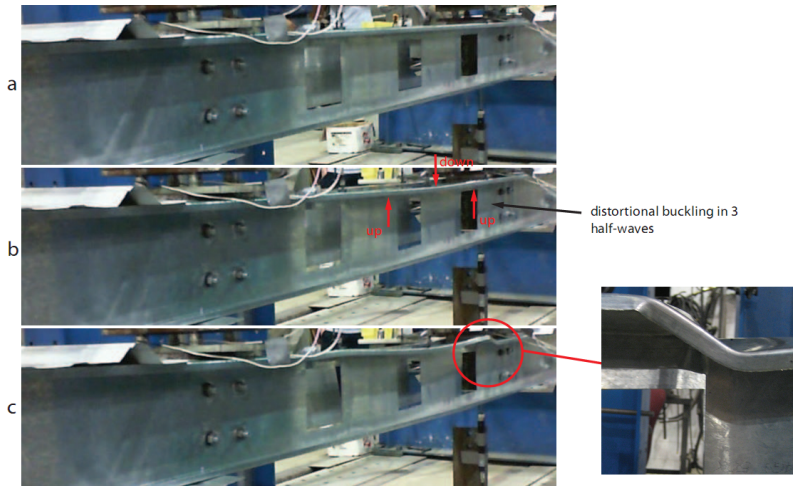

Fig. 3: Load-displacement progression for specimen H0.9-3.1 (a) M=0kNm, (b) M=10.84kNm (peak load) and (c) after collapse M=4.43kNm

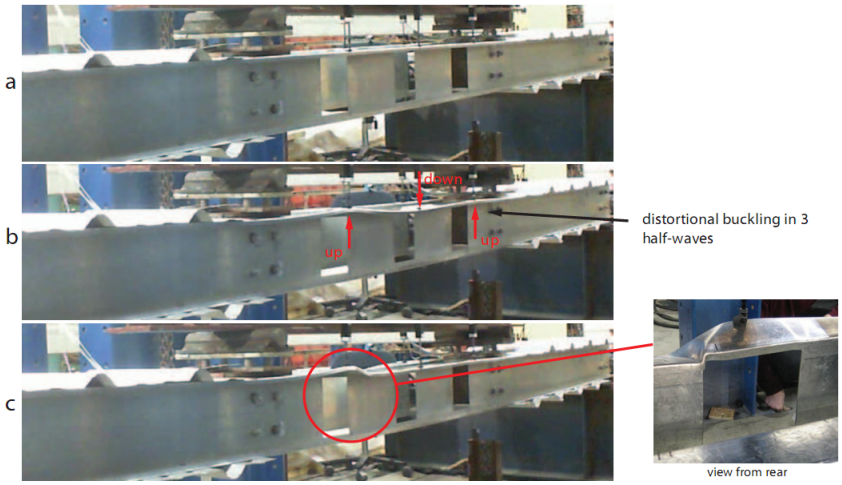

Fig. 4: Load-displacement progression for specimen H0.8-1.2 (a) M=0kNm, (b) M=8.19kNm (peak load) and (c) after collapse M=2.28kNm

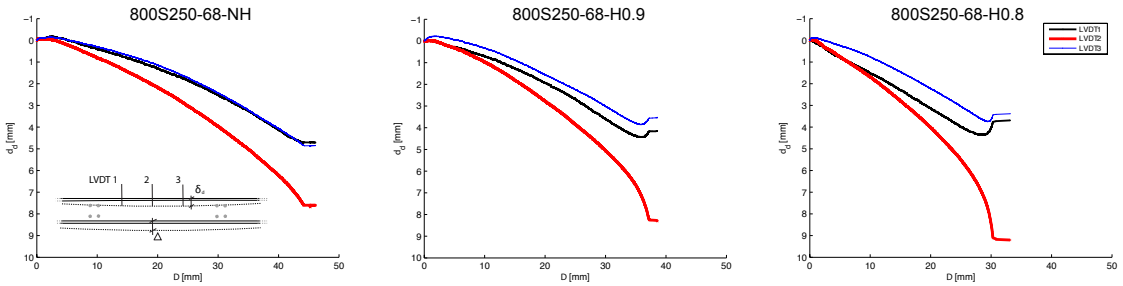

Fig. 5: Joist flange displacement, nonlinearity near failure represents distortional buckling

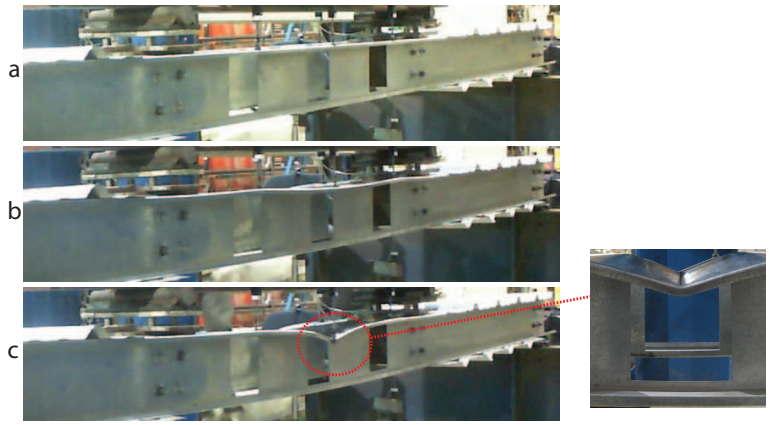

Fig. 6: Load-displacement progression for specimen H0.8-3.2 (a) M=0kNm, (b) M=8.56kNm (peak load) and (c) after collapse M=1.15kNm

3. TEST TO PREDICTION COMPARISON

The tested joist capacities are valuable for evaluating the viability of forthcoming DSM design approach for cold-formed steel joists with holes, summarized in Eqs. (1) to (4) below. These equations are an extension of the existing DSM approach, where the critical elastic buckling moments M_{cre}, $M_{cr\ell}$, and M_{crd} including the influence of holes are calculated with simplified engineering expressions [2,5,10] or thin shell finite element eigen-buckling analysis. Ultimate strength is limited to the net section capacity, M_{ynet}, and an inelastic buckling transition is added from the elastic distortional buckling curve to the yielding regime [4].

The nominal strength of a cold-formed steel beam with holes shall be the minimum of M_{ne}, $M_{n\ell}$, and M_{nd}. The nominal flexural strength, M_{ne}, for lateral-torsional buckling is:

$$M_{ne} = M_{cre} \text{ for } M_{cre} < 0.56\, M_y$$

$$M_{ne} = \frac{10}{9} M_y \left(1 - \frac{10 M_y}{36 M_{cre}}\right) \text{ for } 2.78\, M_y \geq M_{cre} \geq 0.56\, M_y$$

$$M_{ne} = M_y \text{ for } M_{cre} > 2.78\, M_y, \qquad (1)$$

where M_{cre} includes the influence of hole(s).

The nominal flexural strength, $M_{n\ell}$, for local-global buckling interaction is:

$$M_{n\ell} = M_{ne} \leq M_{ynet} \text{ for } \lambda_\ell \leq 0.776$$

$$M_{n\ell} = \left(1 - 0.15\left(\frac{M_{cr\ell}}{M_{ne}}\right)^{0.4}\right)\left(\frac{M_{cr\ell}}{M_{ne}}\right)^{0.4} M_{ne} \quad \text{for } \lambda_\ell > 0.776, \qquad (2)$$

where $\lambda_\ell = (M_{ne}/M_{cr\ell})^{0.5}$, and $M_{cr\ell}$ includes the influence of hole(s).

The nominal flexural strength, M_{nd}, for distortional buckling is:

$$M_{nd} = M_{ynet} \text{ for } \lambda_d \le \lambda_{d1}$$

$$M_{nd} = M_{ynet} - \left(\frac{M_{ynet} - M_{d2}}{\lambda_{d2} - \lambda_{d1}}\right)\left(\lambda_d - \lambda_{d1}\right) \text{ for } \lambda_{d1} < \lambda_d \le \lambda_{d2}$$

$$M_{nd} = \left(1 - 0.22\left(\frac{M_{crd}}{M_y}\right)^{0.6}\right)\left(\frac{M_{crd}}{M_y}\right)^{0.6} M_y \text{ for } \lambda_d > \lambda_{d2}, \quad (3)$$

where $\lambda_d=(M_y/M_{crd})^{0.5}$, $\lambda_{d1}=0.673(M_{ynet}/M_y)$, $\lambda_{d2}=0.673(1.7(M_y/M_{ynet})^{1.7}-0.7)$, M_{crd} includes the influence of hole(s), and

$$M_{d2} = \left(1 - 0.22\left(1/\lambda_{d2}\right)\right)\left(1/\lambda_{d2}\right) M_y . \quad (4)$$

Thin-shell finite element eigen-buckling analysis was performed for each specimen to obtain M_{cre}, M_{crd}, and $M_{cr\ell}$ summarized in Table 4. Tested boundary conditions, measured specimen dimensions, and the presence of holes are included in the elastic buckling parameters, see [11] for details. For the NH specimens, DSM is a conservative predictor of capacity because distortional buckling failure was expected while inelastic local buckling was actually observed, see 'o' symbol in Fig. 7a,b. Distortional buckling capacity is predicted accurately for the H.09 specimens ('Δ' symbol in Fig. 7a), with an average test to predicted mean of 1.06. The DSM prediction is unconservative for the H.08 specimens ('x' symbol in Fig. 7a), where the test-to-predicted mean is 0.85. The unconservative prediction occurs, at least in part, because the flange buckling failure mode above the hole (Figs. 4, 6) was not considered in the elastic buckling parameter calculation or in the development of the inelastic transition to the net section capacity.

Table 4: DSM nominal flexural strength with elastic buckling loads from ABAQUS compared with M_{Test}

Specimen	M_y [kNm]	M_{crd} [kNm]	$M_{cr\ell}$ [kNm]	M_{cre} [kNm]	M_{ne} [kNm]	λ_ℓ	$M_{n\ell}$ [kNm]	λ_d	λ_{d1}	λ_{d2}	M_{d2} [kNm]	M_{nd} [kNm]	M_n [kNm]	M_{Test} [kNm]	M_{test}/M_n
800S250-68-NH-1.1	13.77	15.19	16.66	30.11	13.36	0.90	12.20	0.95	-	-	-	11.122	11.122	12.602	1.13
800S250-68-NH-2.1	13.45	15.41	17.05	29.93	13.08	0.88	12.12	0.93	-	-	-	11.007	11.007	12.512	1.14
800S250-68-NH-3.2	13.70	15.41	17.07	29.41	13.25	0.88	12.23	0.94	-	-	-	11.137	11.137	13.024	1.17
800S250-68-H0.9-1.1	11.98	10.27	16.07	28.17	12.79	0.89	11.71	1.14	0.61	0.88	10.78	9.40	9.40	9.65	1.03
800S250-68-H0.9-2.2	11.90	11.73	16.57	29.13	12.79	0.88	11.82	1.06	0.61	0.89	10.71	9.84	9.84	10.54	1.07
800S250-68-H0.9-3.1	12.32	11.67	16.65	29.02	12.97	0.88	11.95	1.07	0.62	0.85	11.07	9.93	9.93	10.84	1.09
800S250-68-H0.8-1.2	10.67	10.23	16.43	28.56	12.80	0.88	11.80	1.14	0.54	1.18	9.72	9.78	9.78	8.19	0.84
800S250-68-H0.8-2.2	10.66	11.17	16.81	28.71	12.77	0.87	11.87	1.09	0.54	1.17	9.70	9.83	9.83	8.55	0.87
800S250-68-H0.8-3.2	11.16	10.32	16.65	28.44	13.28	0.89	12.15	1.16	0.54	1.17	10.16	10.19	10.19	8.56	0.84

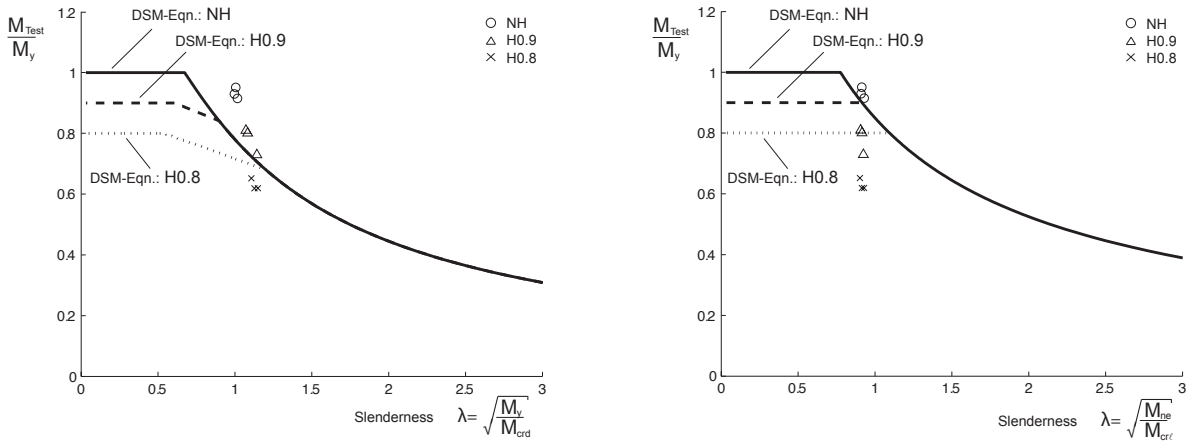

Fig. 7: Comparison of tested capacities to DSM (a) distortional buckling, (b) local buckling predictions

4. CONCLUSIONS

Unstiffened web holes decreased joist capacity and amplified distortional buckling deformation for the cold-formed steel C-section joists considered in this experimental study. The distortional buckling deformation was accompanied by unstiffened strip buckling of the compressed web when hole depth was approximately two-thirds the web depth. When hole depth approached the web depth, unstiffened strip buckling was suppressed and sudden flexural buckling of the compressed flange at the hole occurred. The forthcoming direct strength approach for joists with holes accurately predicted flexural capacity when I_{net}/I_g=0.90, but was unconservative when I_{net}/I_g =0.80. The newly observed flange buckling hole mode caused by large web holes requires further research and consideration.

References

[1] Schafer BW, Peköz T. "Laterally braced cold-formed steel flexural members with edge stiffened flanges", *ASCE Journal of Structural Engineering*, 125(2), 118–127, 1999.

[2] Moen CD, Schafer BW. "Elastic buckling of cold-formed steel columns and beams with holes", *Engineering Structures*, 31(12), 2812-2824, 2009.

[3] AISI-S100-07. *North American Specification for the Design of Cold-Formed Steel Structural Members*, American Iron and Steel Institute, Washington, D.C., 2007.

[4] Moen CD. *Direct Strength Design for Cold-Formed Steel Members with Perforations*, Ph.D. Thesis, Johns Hopkins University, 2008.

[5] Moen CD, Schafer BW. "Extending Direct Strength Design to Cold-formed Beams with Holes", *20th International Specialty Conference on Cold-Formed Steel Structures*, University of Missouri-Rolla, St. Louis, MO, 2010.

[6] Schudlich, A. *Experiments on cold-formed steel joists with unstiffened holes*. Technische Universitat Darmstädt, 2011.

[7] ASTM. *ASTM E8 - 09 / E8M - 09 Standard Test Methods for Tension Testing of Metallic Materials*, 2009.

[8] Moen CD. Dr. Cris Moen's YouTube Channel, <http://www.youtube.com/user/drcrismoen>, accessed April 7, 2011.

[9] Moen CD, Schafer BW. "Elastic buckling of thin plates with holes in compression or bending", *Thin-Walled Structures*, 47(12), 1597-1607, 2009.

[10] Moen CD, Schafer BW. "Direct Strength Design of Cold-Formed Steel Columns with Holes", *2010 Annual Technical Session and Meeting, Structural Stability Research Council*, Orlando, FL, 2010.

[11] von der Heyden A. *Elastic Buckling of Cold-Formed Steel Joists with Unstiffened Holes*, Technische Universitat Darmstädt, 2011.